Journal of Metals, Materials and Minerals, Vol. 32, No. 2, pp. 24-33, 2022

Effects of sputtering power of Ti films on morphology of TiO_2 nanotubes synthesized via anodization process

Pathomporn JUNBANG[1], Chantana AIEMPANAKIT[2], and Kamon AIEMPANAKIT[1,*]

[1] *Department of Physics, Faculty of Science and Technology, Thammasat University, Pathumthani, 12121, Thailand*
[2] *Division of Physics, Faculty of Science and Technology, Rajamangala University of Technology Thanyaburi, Pathumthani, 12110, Thailand*

***Corresponding author e-mail:** akamon@tu.ac.th

Received date:
7 March 2022
Revised date
7 May 2022
Accepted date:
10 May 2022

Keywords:
Ti films;
Sputtering power;
Anodization;
TiO_2 nanotubes

Abstract

In this paper, we aimed to find the sputtering power most suitable for fabricating anodized TiO_2 nanotubes (TNTs) with high dimensions (diameter and length). TNTs were synthesized via anodization of Ti films deposited on a glass substrate at varying sputtering power from 50 W to 200 W. The properties of Ti films such as crystallinity, residual stress, and roughness were investigated, which affected the morphology of TNTs. Sputtering power levels of 150 W and 200 W were suitable for TNTs formation via the anodization process in NH_4F concentrations from 1.0 wt% to 2.5 wt% due to the increased density and crystallinity of Ti films. Boosting the sputtering power to 200 W increases the roughness of the surface, resulting in a decrease in tube diameter and length. Increasing the sputtering power to 200 W also causes the residual stress of the film to be converted from compression to tensile stress, which allows for more TNTs structures to be formed on the film. Nanotubes fabricated on 150 W sputtered films have been proven to be superior to those fabricated at 200 W in every NH_4F concentration in terms of length and diameter. Thus, they are more suitable for applications.

1. Introduction

TiO_2 nanotubes (TNTs) have garnered much interest due to their wide range of applications in several fields such as optical physics and biomedicine. Owing to their high surface-to-volume ratio and charge transport property, they can improve the performance of various processes such as gas sensing [1], photovoltaic activity [2], and photocatalysis [3], as well as the surface coating of medical implants, localized drug delivery systems [4], and the fire retardancy of textile products [5,6]. These processes have been improved by integrating zero to two-dimensional TiO_2 nanomaterials [7] such as nanoparticles [8], nanowires [9], nanorods [10], and nanotubes [11]. Particularly, the efficiency of dye-sensitized solar cells increases when TiO_2 nanotubes are integrated. Nanotubes are widely used as anodes in solar cells due to their highly-ordered structures and high surface area, which transport a higher number of electrons faster than nanoparticles. Nanotubes can be made from several materials such as ZnO, MgO, CdS, etc. However, TiO_2 is favored due to its low cost, non-toxicity, and biocompatibility, making it useful in prostheses and implants [12]. Several methods for TNTs synthesis have been developed such as sol-gel, hydrothermal and solvothermal, anodization, etc. Among the methods for the large-scale production of TNTs, anodization in fluoride-containing electrolytes is the best because it is the most environmental-friendly and the rate of chemical dissolution is very high, making the process much faster [13,14]. Additionally, this method allows for the easy control of the dimensions, surface area, and density of nanotubes by adjusting related variables such as voltage, water content, and fluoride concentration in electrolytes [12].

Either Ti films or Ti foils can be used as substrates in anodization to create nanotubular structures. However, TNTs synthesized from pre-made Ti foil are opaque and also unable to withstand high stress, making them ill-suited for dye-sensitized solar cells, with a higher tendency for device failure [15]. Furthermore, Ti foil typically has a thickness of 0.1 mm to 2.0 mm, so synthesis from Ti foil to TNTs-based devices causes them to be large and energy-inefficient [16]. Several researchers have studied the method to control the morphology of anodized thin films, and it has been demonstrated that the sputtering and anodization parameters affect the resulting morphology of TNTs films. Chappanda *et al* [16] showed that high film density is significant in achieving a tubular structure due to electric field uniformity across the film surface. Jaafar *et al* [17] demonstrated that nanotube lengths increase with the concentration of NH_4F electrolyte. However, the results of these studies were occasionally contradictory. For instance, Pasikhani *et al* [18] demonstrated that length, diameter, and wall thickness increased with anodization voltage. In contrast, Alsammarraie *et al* [19] provided results where the same variables did not exhibit consistent correlations with anodization voltage. During Ti film deposition with magnetron sputtering, changes in the sputtering parameters can affect the morphology and physical quantities of the Ti film. This is because changes in sputtering power, substrate temperature, and gas pressure can change the residual stress of the film [16]. The work of Liao *et al* revealed that higher residual stress increases pore formation during anodization

[20]. However, Chappanda *et al* [16] showed that residual stress has no effect on the morphology of anodized films. These results also raise doubts about the effects of the sputtering variable on the TNTs structure.

In this work, the effects of the sputtering power of Ti films on the morphologies of TNTs films after anodization were investigated. We considered that increased sputtering power caused changing crystallinity, surface roughness, and residual stress in Ti films, which affected the morphology of Ti and TNTs including the diameter, length, and density of the tubes. In addition, various concentrations of NH_4F in the anodization process were provided to compare the morphology of TNTs at different sputtering power of the Ti films.

2. Experimental details

2.1 Ti film deposition

Ti films were deposited on glass substrates (2.50 $cm^2 \times 3.00$ cm^2) by using the DC magnetron sputtering technique from a 99.995% pure Ti target (2 in. diameter and 0.25 in. thick, Kurt J. Lesker). The distance between the target and substrate was 8.0 cm. The sputtering chamber was pumped down with a rotary pump and diffusion pump to a base pressure of 5×10^{-5} mbar. Subsequently, argon gas was fed into the chamber at a flow rate of 15 sccm (standard cubic centimeters per minute) while the working pressure was kept constant at 1×10^{-2} mbar. The sputtering power was varied from 50 W to 250 W to provide differences in the Ti structure. The deposition rates corresponding to each sputtering power are reported in Table 1. The thickness of the Ti films was found to be approximately 1.0 μm.

2.2 TNTs synthesis

The adonization process was used to synthesize TNTs. Prior to anodization, the Ti films (1.0 $cm^2 \times 2.0$ cm^2) were sequentially cleaned by sonicating in deionized water, 2-propanol, and acetone for 15 min each. Anodization was conducted under a constant voltage of 30 V supplied into a two-electrode cell with Ti film serving as the anode and lead as the cathode, which were 4.00 cm apart. The electrodes were immersed in an electrolyte consisting of glycerol ($C_3H_8O_3$, GR), H_2O, and NH_4F. The Ti films were anodized with 1.0 wt% to 2.5 wt% NH_4F as shown in Table 2. After anodization, the TNTs films were rinsed in deionized water for 30 min to remove any debris covering the top of the nanotubes and then dried in hot air. The reactions of anodization are explained in Section 2.4.

2.3 Film characterizations

The morphologies of films, both pre- and post-anodization, were examined using field emission scanning electron microscopy (FE-SEM, Tescan/Mira3, Czech Republic). The crystallographic structures before anodization were determined by X-ray diffraction (XRD, Bruker, D2 Phaser) in the 2θ range of 20° to 70° using CuKα radiation with a wavelength of λ=1.5406 Å at room temperature. X-ray tubes were operated at 30 kV and 10 mA. The surface roughness of the Ti films was analyzed using atomic force microscopy (AFM, JPK Instruments, Nano Wizard Ultras) in AC mode at ambient temperature. Root mean square (Ra) surface roughness was obtained by scanning over an area of 5 $\mu m^2 \times 5$ μm^2. The nanostructure and values of d spacing of the Ti films were obtained using transmission electron microscopy (TEM, JEM-2100Plus Electron Microscope).

2.4 Mechanism of TNTs formation via anodization

The formation of self-ordered nanotubes with thin walls and a high aspect ratio relies on competition between the oxidation of Ti, which produces TiO_2, and the chemical dissolution of TiO_2 [21]. Films sputtered under the conditions in Table 1 were anodized in electrolytes whose compositions are reported in Table 2. TiO_2 was first formed on the film's surface [22,23]. Ti atoms were oxidized by the applied voltage, producing Ti^{4+}, as shown in reaction (1).

$$Ti \rightarrow Ti^{4+} + 4e^- \quad (1)$$

Table 1. Deposition conditions.

Sputtering power (W)	Argon pressure (mtor)	Deposition rate ($nm \cdot s^{-1}$)	Argon flow rate (sccm)
50	1×10^{-2}	0.22	15
100	1×10^{-2}	0.39	15
150	1×10^{-2}	0.71	15
200	1×10^{-2}	1.00	15

Table 2 Anodizing conditions of Ti films sample groups.

Sputtering Power		Anodization parameters			
Sample group	Power (W)	GR electrolyte (60 mL)		Voltage (V)	Time (min)
		NH_4F (wt%)	H_2O (wt%)		
(SGI)	50 W 100 W 150 W 200 W	2.5	5	30	60
(SGII)	150 W 200 W	1, 1.5, 2, 2.5	5	30	60

Ti^{4+} was then combined with O^{2-} from the breakdown of H_2O in field-assisted oxidation processes, producing TiO_2. The breakdown of H_2O, the reduction of O, and the production of the TiO_2 layer above the Ti films are shown in reactions (2), (3), and (4), respectively.

$$2H_2O \rightarrow O_2 + 4e^- + 4H^+ \quad (2)$$

$$2O_2 + 4e^- \rightarrow 4O^{2-} \quad (3)$$

$$2Ti^{4+} + 4O^{2-} \rightarrow 2TiO_2 \quad (4)$$

Furthermore, O^{2-} can pass through the TiO_2 layer to combine with the Ti^{4+} between the Ti film and TiO_2 layer, thus forming TiO_2 beneath the surface/electrolyte interface. At the cathode, the hydrogen ions from (2) combine with electrons from the cathode to form H_2. The electric field weakens the Ti-O bonds of the TiO_2 molecules, assisting the etching of TiO_2 by F^- from NH_4F. Nanopores are formed through this field-assisted dissolution. At the same time, F^- can pass through the surface/ electrolyte interface to etch TiO_2 underneath the surface. The field-assisted dissolution processes are shown in reaction (5).

$$TiO_2 + 6F^- + 4H^+ \rightarrow [TiF_6]^{2-} + H_2 + H_2O \quad (5)$$

The production of $[TiF_6]^{2-}$ can also occur when Ti^{4+} from underneath the TiO_2 layer moves towards the electrolyte or when F^- moves towards the titanium metal under the electric field influence. Reaction (6) describes their combinations.

$$Ti^{4+} + 6F^- \rightarrow [TiF_6]^{2-} \quad (6)$$

The increasing presence of H^+ in the electrolyte and TiO_2^{2+} in the film due to reactions (2), (7), and (8) increases the electric field intensity [24], causing more F^- to migrate to and accumulate at these sites, which, in turn, increases the rate of field-assisted dissolutions, forming voids between the nanotubes.

$$Ti^{4+} + 4H_2O \rightarrow Ti(OH)_4 + 4H^+ \quad (7)$$

$$Ti(OH)_4 \rightarrow TiO^{2+} + O_2 + 4H^+ + 6e^- \quad (8)$$

After the oxidization and etching processes have continued for some time, the rates of both reactions become equal. When equilibrium is reached, the thicknesses of the barriers between the oxide layer and Ti metal are equal and remain constant as the tubes continue to deepen [22].

3. Results and discussion

3.1 Effects of sputtering power on Ti film

The FE-SEM image in Figure 1 shows top and side views of Ti thin films sputtered at different sputtering power on substrates at room temperature. The energy of Ar^+ plays a vital role in determining the final morphology of the film as energy is transferred from Ar^+ to the sputtered Ti atoms upon collision with the Ti target. The results show that grain size increased with increased sputtering power. At a sputtering power of 50 W, Ti film cannot show any clear granular structure due to the adatoms being unable to efficiently nucleate because they lack sufficient energy to diffuse on the surface to

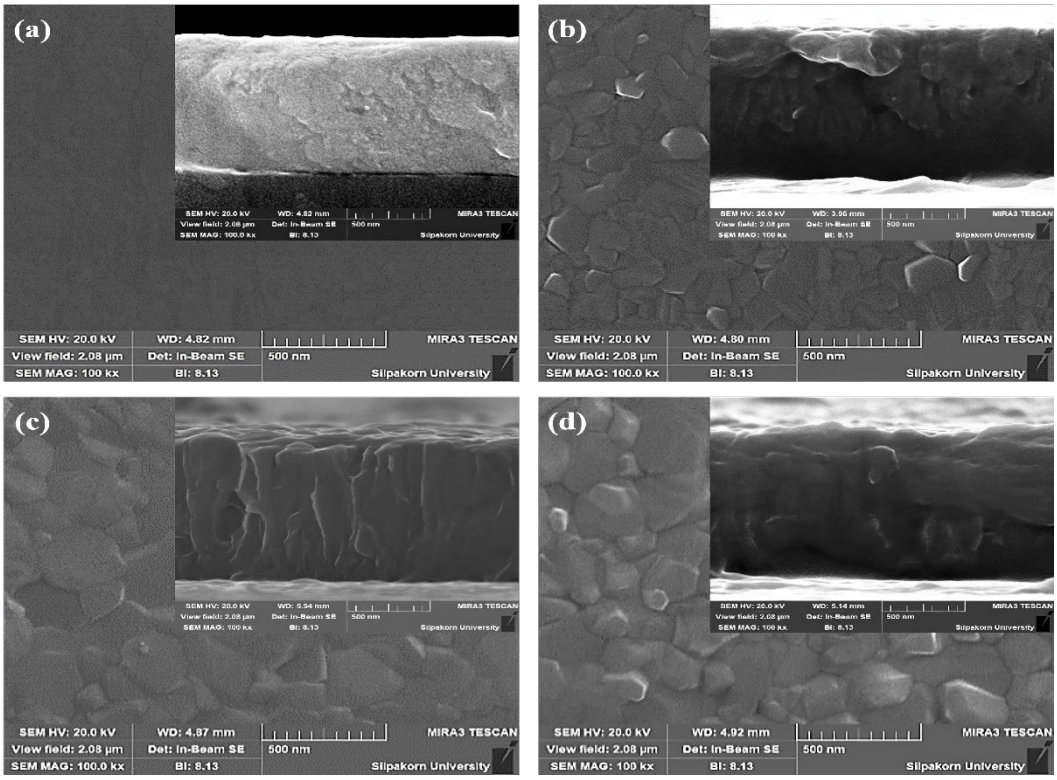

Figure 1. Top and side views of FE-SEM image of sputtered Ti thin films at sputtering power of a) 50 W, b) 100 W, c) 150 W, and d) 200 W.

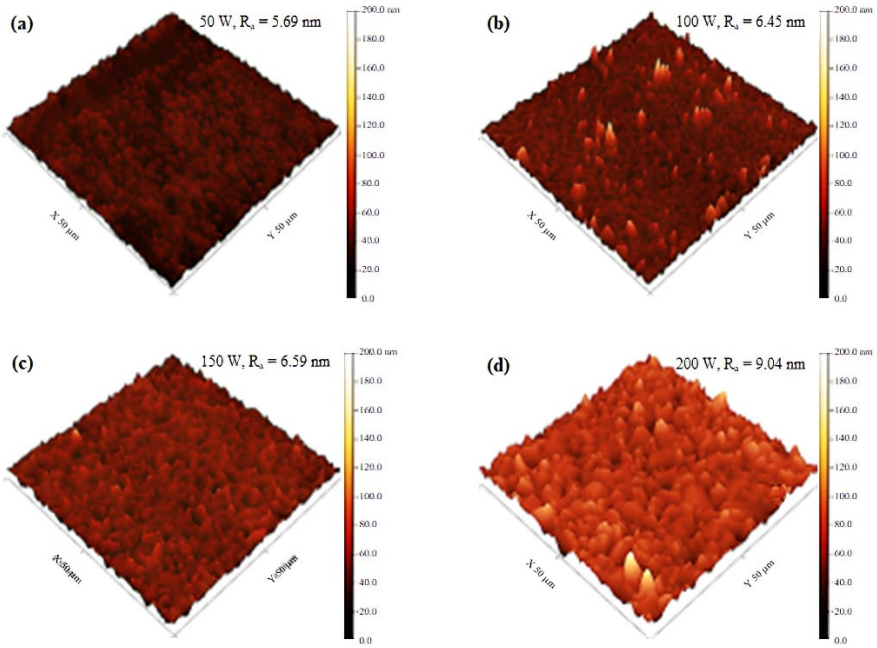

Figure 2. 3D-AFM images and roughness of the Ti films sputtered with different sputtering powers of a) 50 W, b) 100 W, c) 150 W, and d) 200 W.

a suitable position. At higher sputtering power, nucleation can occur as the adatoms now have more energy for diffusion on the surface to form clusters and islands of Ti. Mobility aids in the merging of the islands that have formed and consequently increases grain size and densification. The additional energy of Ti atoms also serves to increase the density of the film when the atoms bombarding have sufficient energy to be incorporated into small spaces in the film normally inaccessible under thermal equilibrium [25,26], thus promoting nucleation and densification (see Table 3). Lastly, the increase in deposition rate also increases density [27]. In terms of surface roughness, it can be qualitatively observed that surface roughness increases with sputtering power, with the film sputtered at 200 W being the roughest and having a more noticeably faceted surface, as shown in Figure 2, in agreement with the previous work of Liao *et al* [28]. From the side view, it can be observed in Figures 1(b) and 1(c) that the films have columnar structures when individual grains become perceptible. However, the columnar structure disappears at 200 W, leading to increased densification as the gaps between columns disappear.

3.2 Crystallographic structure

Figure 3 shows the XRD patterns before anodization of the Ti films sputtered with different levels of sputtering power. According to the XRD, all films exhibited the characteristics of Ti crystals in the α phase. Bragg reflections corresponding to the (100), (101), and (002) orientations were observed, with (002) being the dominant diffraction peak for Ti in accordance with the standard XRD database (PDF card on 01-086-2608). All diffraction peaks increased in intensity as the sputtering power was increased, likely due to the high mobility of adatoms aiding the nucleation process. Consequently, films sputtered with 50 W sputtering power remain amorphous because of the low mobility of adatoms. XRD data were used in the calculation of grain size using the Scherrer equation as equation (9) with the shape factor of 0.92:

$$D = \frac{0.92\lambda}{FWHM\ \cos\theta} \quad (9)$$

where λ is the wavelength of the X-ray, and FWHM is the full width at half maximum. The results are reported in Figure 4. Increasing the sputtering power from 50 W to 200 W resulted in a significant increase in grain size due to nucleation.

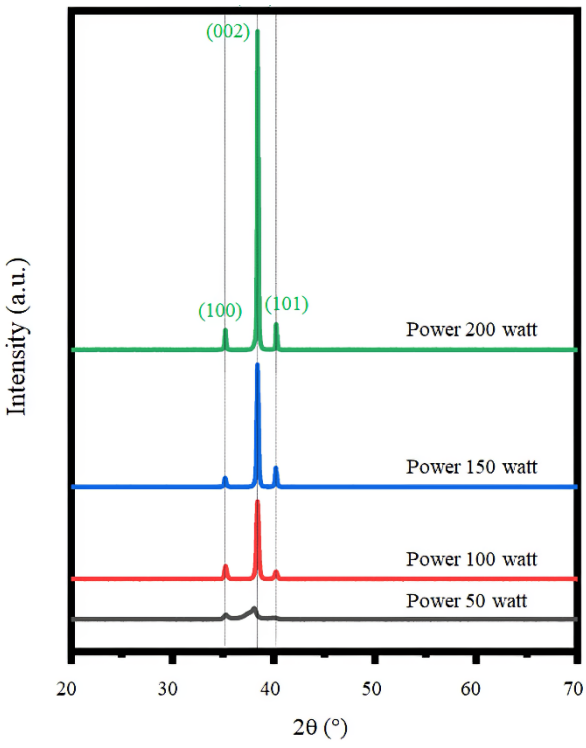

Figure 3. XRD patterns of Ti films prepared at different sputtering powers.

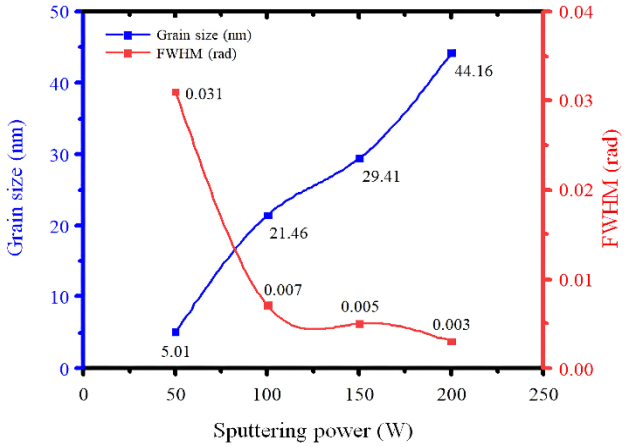

Figure 4. FWHM and grain size with respect to sputtering power.

Diffraction peak (002) is the most favored orientation due to its surface free energy, which is the lowest [30]. If adatoms have enough mobility after arriving on the substrate, the film will grow along its most energetically favorable planes [31]. For this reason, the growth of peak (002) is observed as a result of increased sputtering power.

Residual stress occurred in the film during deposition, which was calculated from the crystallographic structure by using equation (10) [31]:

$$\sigma = \frac{E_y(d-d_0)}{\tau d_0} \qquad (10)$$

where Ey is the Young modulus, d is the crystallite plane spacing that can be obtained from TEM images or diffraction patterns, d0 is the standard crystallite spacing for peak (002) for unstressed films (PDF card on 01-086-2608), and τ is the Poisson ratio. For titanium, Ey = 110 GPa and τ = 0.31 [32]. Table 3 reports the residual stress of the Ti films for all sputtering power levels. Diffraction patterns from TEM images in Figure 5 were used to determine the d spacing of the films. In this study, the residual stress was caused by the substrate temperature and the energy of the adatoms varying with different sputtering powers. As reported in Table 3, the residual stress of the Ti films was compressive at first, then became tensile as the sputtering power increased. Compressive stress developed due to atomic implantation. Energetic atoms were implanted near the film surface, which resulted in the deformation of this layer in the film.

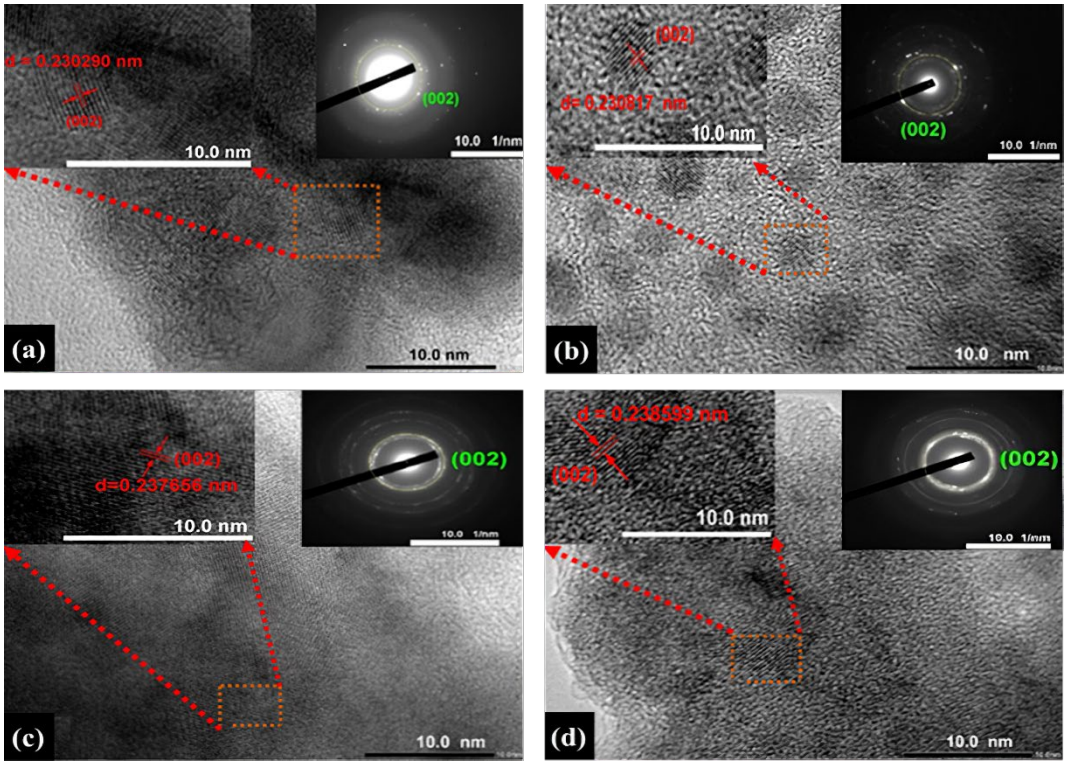

Figure 5. TEM images of Ti films at sputtering power of a) 50, b) 100 W, c)150 W, and d) 200 W and the insets in upper-right corner are corresponding to the diffraction patterns.

Table 3. Density, residual stress, and crystallite plane spacing (d) measured in TEM images of various puttering power of Ti films.

Sputtering power (W)	Density ($g \cdot cm^{-3}$)	(002) plane space (nm)	Residual stress (GPa)
50	4.45	0.230290	-5.73093
100	4.56	0.230817	-4.93079
150	4.62	0.237656	5.43579
200	4.72	0.238599	6.86629

However, deformation was constrained by the underlying materials, giving rise to compression. The reduction of compressive stress and the increase in tensile stress occur because there are fewer gaps or voids within the film as the film densifies due to the increase of sputtering power, which reduces the chances of atoms being implanted [33]. Furthermore, the closing of gaps means that the distance between grains becomes closer, strengthening the interatomic force and consequently the stretching effect [13]. Figure 6 shows the correlation between residual stress and grain size. The increase in grain size accompanies the densification of the film along with gap reduction. Therefore, it is observed that residual stress becomes tensile as grain size increases

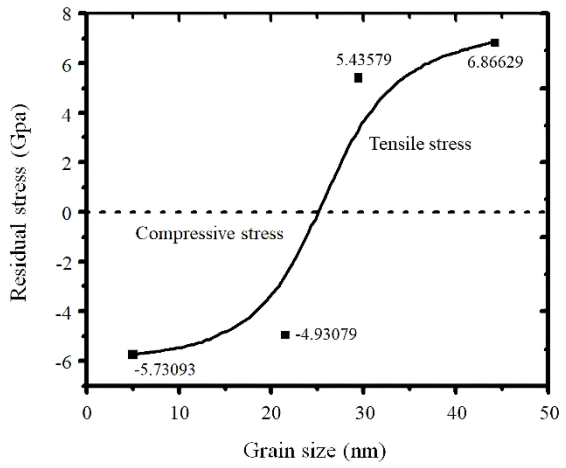

Figure 6. Residual stress as a function of grain size.

3.3 Effect of sputtering power on the nanotubular structure

Figure 7 shows the top and side views from FE-SEM images of the Ti films after anodization. The nanoporous structure started formation from the Ti film deposited at a sputtering power of 50 W. Only short nanotubular structures are formed on the Ti with a sputtering power of 100 W. The tubular structure becomes more apparent as the sputtering power is increased due to the densification of the Ti film [34]. Therefore, sputtering power levels of 150 and 200 W will be used to further study the effect of NH_4F concentration on nanotube structures.

3.4 Effects of electrolyte composition on tubularity

Sputtered Ti films at 150 W and 200 W were anodized in electrolytes with various NH_4F concentrations of 1.0, 1.5, 2.0, and 2.5 wt%. The top and side views from FE-SEM images of the sputtering power of Ti films at 150 W and 200 W are shown in Figures 8 and Figure 9, respectively. As shown in Figure 8, it can be observed that an NH_4F concentration of 1 wt% is not able to sufficiently dissolve the walls of the nanotubes, resulting in narrow openings of the tubes. The increase in NH_4F concentrations modified well in this regard, with all anodized Ti films in these concentrations having longer diameters. In addition, for the Ti films anodized at a voltage higher than 10 V, bridges of interlocking nanotubes exist, which are the result of the partial dissolution of adjacent oxide rings and give the nanotubes their bamboo-like structures [35]. However, it has also been observed that particular electrolyte compositions give rise to such a structure [36].

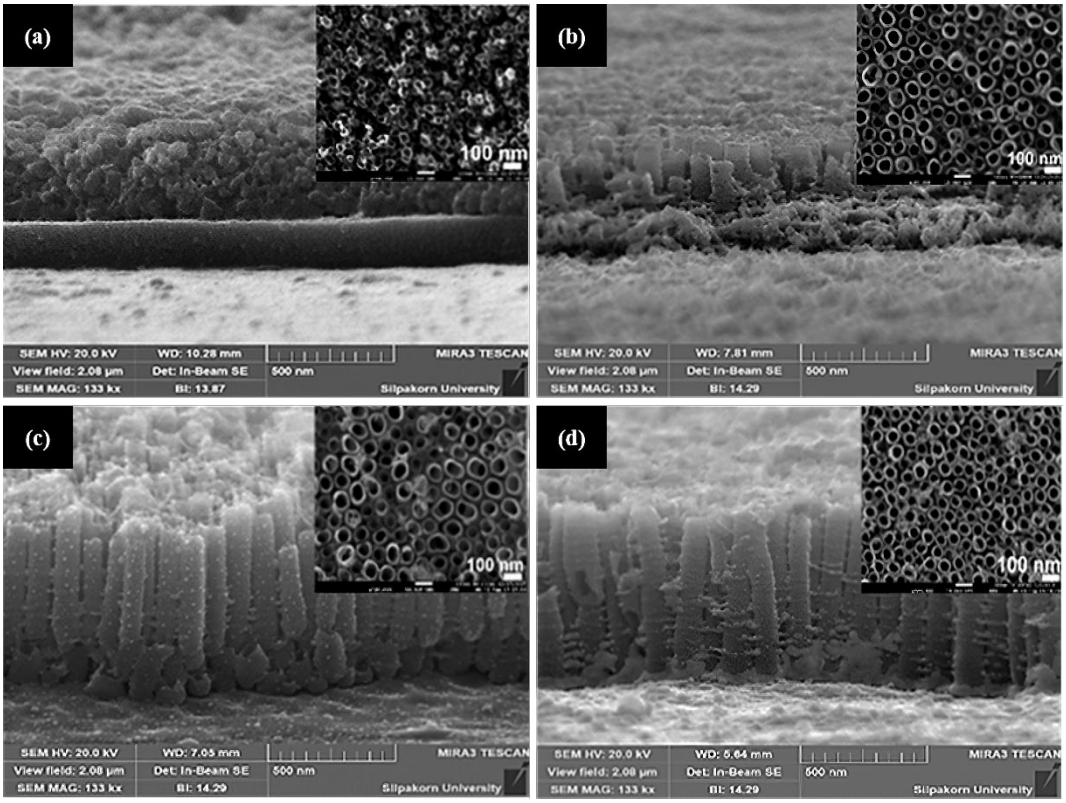

Figure 7. Top views and cross-sections of FE-SEM images of anodized Ti films with sputtering power of a) 50 W, b) 100 W, c) 150 W, and d) 200 W.

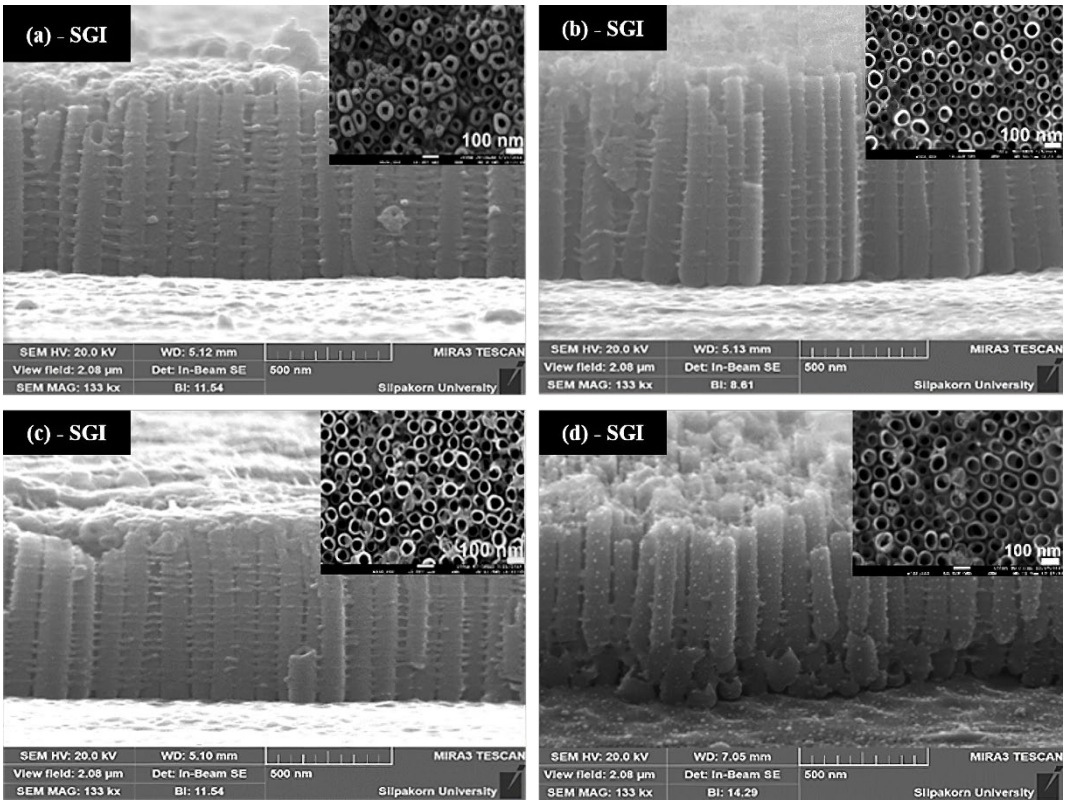

Figure 8. The side and top views of FE-SEM images of anodized Ti films at sputtering power of 150 W (SGI) in various NH_4F concentrations of a) 1.0 wt%, b) 1.5 wt%, c) 2.0 wt%, and d) 2.5 wt%.

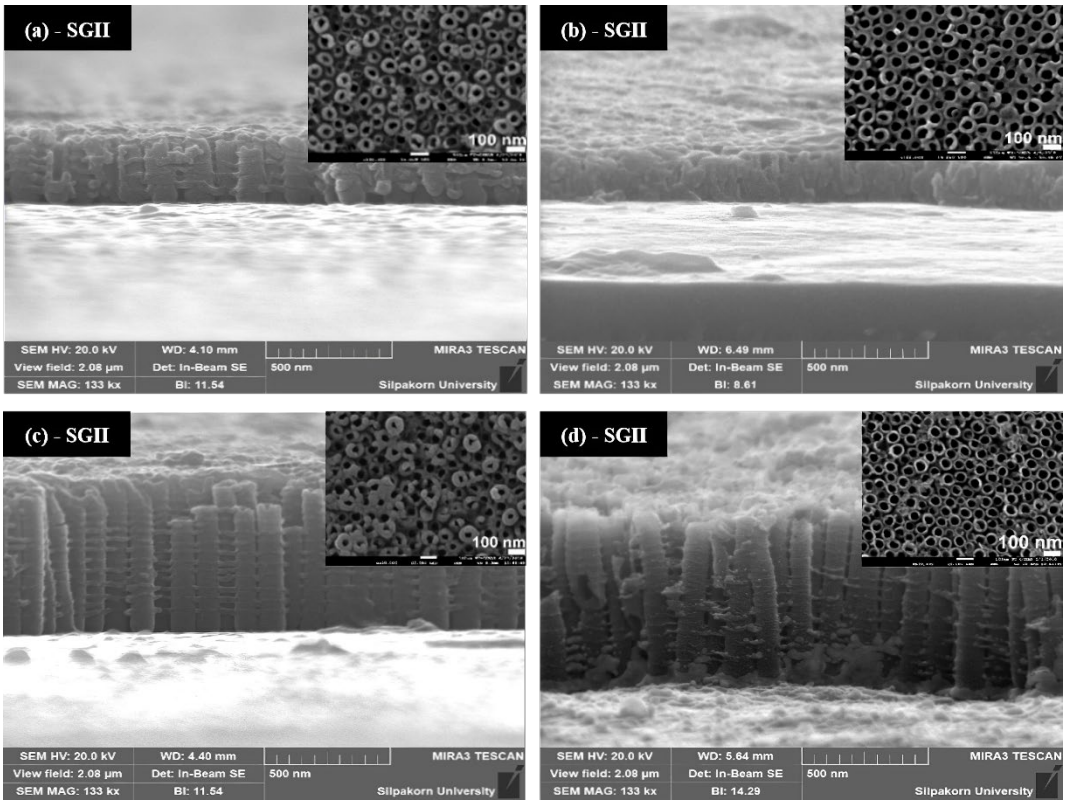

Figure 9. The side and top views of FE-SEM images of anodized Ti films at sputtering power of 200 W (SGII) in various NH_4F concentrations of a) 1.0 wt%, b) 1.5 wt%, c) 2.0 wt%, and d) 2.5 wt%.

In Figure 9, more oxide remains around the openings after ultrasonic cleaning. Because the higher NH_4F content enhances the dissolution of the oxide [37], only a 2.5 wt% concentration is necessary to dissolve the oxide around the rims of the openings. Considering the sputtering power of 150 W and 200 W, when anodized Ti films at an NH_4F concentration of 1 wt% showed nanotubular structures, they were different in diameter and length. The diameter and length of TNTs synthesized from the sputtering power of 150 W were longer than those of 200 W, as shown in Figures 10(a) and 10(b). At a sputtering power of 150 W and anodization in NH_4F concentrations of 1, 1.5, 2, and 2.5 wt%, diameters of TNTs were 37.59, 52.39, 48.58, and 59.63 nm, while the lengths of TNTs were 824.84, 877.79, 805.94, 757.81 nm, respectively. For sputtering power of 200 W, diameters of TNTs were 35.98, 45.33, 36.87, and 47.52 nm, while the lengths of TNTs were 294.08, 186.33, 587.61, and 753.06 nm, respectively. Therefore, the larger dimensions of TNTs for sputtering power of 150 W indicated higher surface area than 200 W [38]. Additionally, a sputtering power of 200 W exhibited higher numbers of nanotubes per unit area, according to Figure 10(c). For NH_4F concentrations of 1, 1.5, 2, and 2.5 wt%, sputtering power of 150 W showed tube densities of 114.81, 135.19, 137.04, and 95.37 tubes/μm^2, respectively, while sputtering power of 200 W exhibited tube densities of 171.31, 146.29, 138.89, and 141.66 tubes/μm^2, respectively.

A previous study found that the grain size of Ti films did not significantly affect the anodized film structure, but film density was the main factor [13]. Therefore, it was expected that the sputtering power of 200 W, which had higher density Ti films, would have more well-ordered and longer nanotube arrays than the 150 W films because of this higher density. However, it can be seen in Figure 10(a-b) that the lengths and diameters of TNTs for a sputtering power of 200 W were significantly shorter than those of 150 W in every concentration. The shorter TNTs layer at a sputtering power of 200 W was possible to obtain because field-assisted chemical dissolution was directed by the electric field [39]. Film roughness can disrupt the uniformity of the electric field across the film surface, causing the films to be etched in a random manner, which can damage the structure of the nanotubes [40]. Consequently, a smooth surface increases the growth rate of TNTs since the uniform electric field aids the ion transport to the anodic film, causing the lengths and diameters of TNTs to be longer when synthesized from the sputtering power of 150 W films [41]. Figure 10(c) shows that the density of nanotubes fabricated on Ti with a sputtering power of 200 W was greater than that of 150 W under every NH_4F concentration. This is due to the higher residual stress of the Ti film at a sputtering power of 200 W, which facilitated initial pore formation [20]. Even though a higher count of nanotubes can be fabricated using the sputtering power of 200 W films, their shorter length and diameter make them less unsuitable for use in applications. Therefore, the sputtering power of 150 W with TNTs of larger dimensions was preferable.

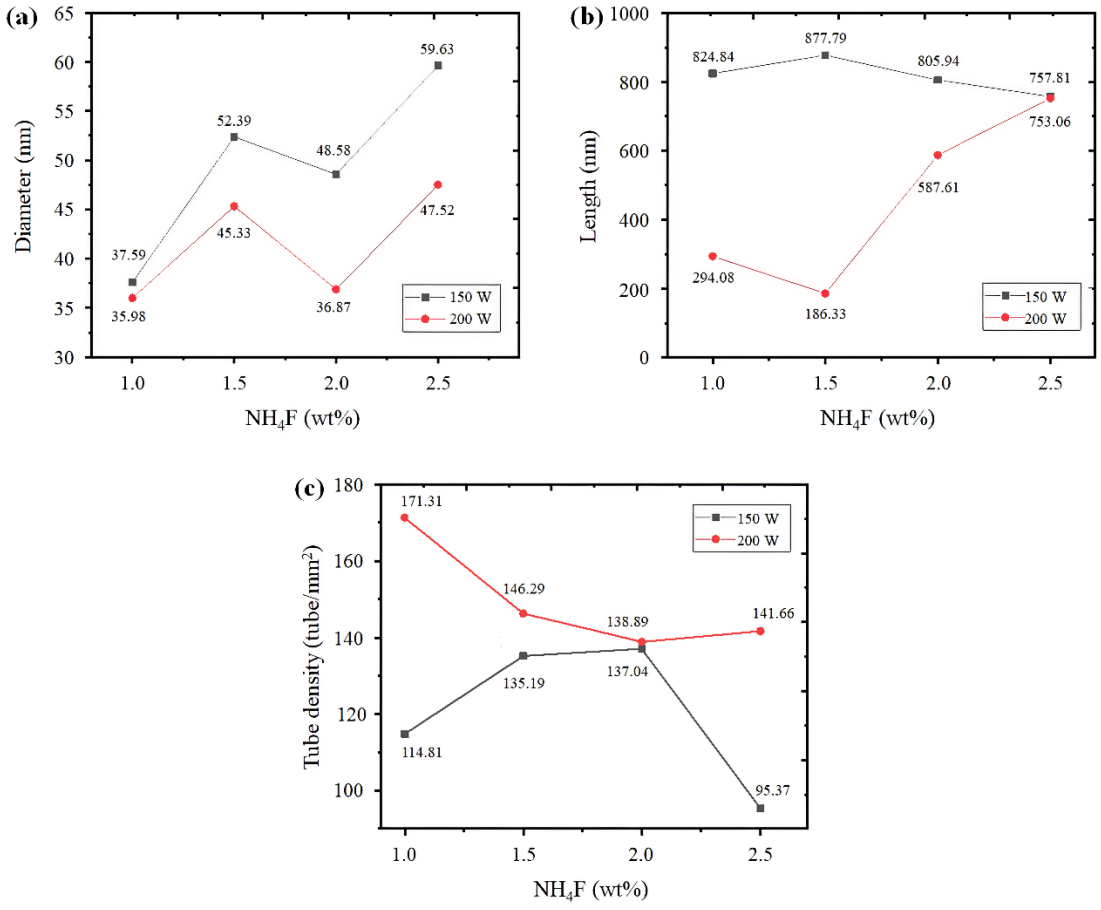

Figure 10. Diameter a), length b), and tube density c) of nanotubes at sputtering power of 150 W and 200 W in various NH_4F concentrations.

4. Conclusions

TNTs were fabricated from Ti thin films deposited with varying sputtering power levels. TNTs tubularity increased with increasing sputtering power at 150 W and 200 W. Higher sputtering power enhanced the density of Ti films, being necessarily suitable for the formation of nanotubes with the anodization process. The surface roughness and residual stress of Ti films were also important factors in achieving tubular structures. The results exhibited that the highest length and diameter of TNTs were synthesized from the sputtered Ti film at a sputtering power of 150 W, which showed smoother surfaces than at 200 W. Moreover, residual stress facilitated initial pore formation, increasing tube density. Therefore, a greater density of TNTs was fabricated on sputtered Ti films at a sputtering power of 200 W, which showed higher residual stress. Despite its higher count of nanotubes, long and wide nanotube dimensions at a sputtering power of 150 W was more preferable in applications due to higher surface area.

References

[1] Y. Kwon, H. Kim, S. Lee, I.-J. Chin, T.-Y. Seong, W. I. Lee, and C. Lee, "Enhanced ethanol sensing properties of TiO_2 nanotube sensors," *Sensors and Actuators B: Chemical*, vol. 173, pp. 441-446, 2012.

[2] P. Roy, S. P. Albu, and P. Schmuki, "TiO_2 nanotubes in dye-sensitized solar cells: Higher efficiencies by well-defined tube tops," *Electrochemistry Communications*, vol. 12, no. 7, pp. 949-951, 2010.

[3] Y. S. Sohn, Y. R. Smith, M. Misra, and V. (Ravi) Subramanian, "Electrochemically assisted photocatalytic degradation of methyl orange using anodized titanium dioxide nanotubes," *Applied Catalysis B: Environmental*, vol. 84, no. 3-4, pp. 372-378, 2008.

[4] S. Jafari, B. Mahyad, H. Hashemzadeh, S. Janfaza, T. Gholikhani, and L. Tayebi, "Biomedical Applications of TiO_2 Nanostructures: Recent Advances," *International Journal of Nanomedicine*, vol. 15, pp. 3447–3470, 2020.

[5] E. M. Elsayed, N. F. Attia, and L. A. Alshehri, "Innovative Flame Retardant and Antibacterial Fabrics Coating Based on Inorganic Nanotubes," *Chemistry Select*, vol. 5, no. 10, pp. 2961-2965, 2020.

[6] N. F. Attia and M. Mousa, "Synthesis of smart coating for furniture textile and their flammability and hydrophobic properties," *Progress in Organic Coatings*, vol. 110, pp. 204-209, 2017.

[7] N. F. Attia, "Organic nanoparticles as promising flame retardant materials for thermoplastic polymers," *Journal of Thermal Analysis and Calorimetry*, vol. 127, no. 3, pp. 2273-2282, 2016.

[8] H. K. Sung, Y. Lee, W. H. Kim, S.-J. Lee, S.-J. Sung, D.-H. Kim, and Y. S. Han, "Enhanced Power Conversion Efficiency of Dye-Sensitized Solar Cells by Band Edge Shift of TiO_2 Photoanode," *Molecules*, vol. 25, no. 7, p. 1502, 2020.

[9] X. Yu, H. Wang, Y. Liu, X. Zhou, B. Li, L. Xin, Y. Zhou, and H. Shen,"One-step ammonia hydrothermal synthesis of single crystal anatase TiO_2 nanowires for highly efficient dye-sensitized solar cells," *Journal of Materials Chemistry A*, vol. 1, no. 6, pp. 2110-2117, 2013.

[10] J. Wang, S. Qu, Z. Zhong, S. Wang, K. Liu, and A. Hu, "Fabrication of TiO_2 nanoparticles/nanorod composite arrays via a two-step method for efficient dye-sensitized solar cells," *Progress in Natural Science: Materials International*, vol. 24, no. 6, pp. 588-592, 2014.

[11] F. Mohammadpour and M. Moradi, "Double-layer TiO_2 nanotube arrays by two-step anodization: Used in back and front-side illuminated dye-sensitized solar cells," *Materials Science in Semiconductor Processing*, vol. 39, pp. 255-264, 2015.

[12] A. Abd Aziz, "Synthesis and Characterization of TiO_2 Nanotube Using Electrochemical Anodization Method," *International Journal of Engineering Technology and Sciences*, vol. 5, no. 3, pp. 132-139, 2018.

[13] B. Li, X. Gao, H.-C. Zhang, and C. Yuan, "Energy Modeling of Electrochemical Anodization Process of Titanium Dioxide Nanotubes,"*ACS Sustainable Chemistry & Engineering*, American Chemical Society (ACS), vol. 2, no. 3, pp. 404-410, 2013.

[14] J. M. Macak, H. Tsuchiya, S. Berger, S. Bauer, S. Fujimoto, and P. Schmuki, "On wafer TiO_2 nanotube-layer formation by anodization of Ti-films on Si," *Chemical Physics Letters*, vol. 428, no. 4-6, pp. 421-425, 2006.

[15] Y. Tang, J. Tao, Z. Dong, J. T. Oh, and Z. Chen, "The formation of micrometer-long TiO_2 nanotube arrays by anodization of titanium film on conducting glass substrate," *Advances in Natural Sciences: Nanoscience and Nanotechnology*, vol. 2, no. 4, p. 045002, 2011.

[16] K. N. Chappanda, Y. R. Smith, L. W. Rieth, P. Tathireddy, M. Misra, and S. K. Mohanty, "Effect of sputtering parameters on the morphology of TiO_2 nanotubes synthesized from thin Ti film on Si substrate," *IEEE Transactions on Nanotechnology*, vol. 14, no. 1, pp. 18-25, 2015.

[17] H. I. Jaafar, A. M. A. Alsammerraei, and H. H. Hamdan, "Study of the effect of NH_4F concentration on the sutrcture of electrochemically prepared TiO_2 nanotubes," *Iraqi Journal of Science*, vol. 53, no. 2, pp. 827-831, 2012.

[18] J. V. Pasikhani, N. Gilani, and A. E. Pirbazari, "The effect of the anodization voltage on the geometrical characteristics and photocatalytic activity of nanotube arrays," *Nano-Structures & Nano-Objects*, vol. 8, pp. 7-14, 2016.

[19] A. M. A. Alsammarraei, H. I. Jaafar, K. N. Abed, "The role of anodizing potentials in making TiO_2 nanotubes in (ethylene glycol/NH_4F /water) electrolyte," *Archives of Applied Science Research*, vol. 6, no. 2, pp. 115-121, 2014.

[20] M. W. Liao and C. K. Chung, "The role and effect of residual stress on pore generation during anodization of aluminium thin films," *Corrosion Science*, vol. 74, pp. 232-239, 2013.

[21] G. K. Mor, O. K. Varghese, M. Paulose, N. Mukherjee, and C. A. Grimes, "Fabrication of tapered, conical-shaped titania nanotubes," *Journal of Materials Research*, vol. 18, no. 11, pp. 2588-2593, 2003.

[22] J. M. Macak, H. Tsuchiya, A. Ghicov, K. Yasuda, R. Hahn, S. Bauer, and P. Schmuki, "TiO_2 nanotubes: Self-organized

electrochemical formation, properties and applications," *Current Opinion in Solid State and Materials Science*, vol. 11, no. 1-2, pp. 3-18, 2007.

[23] K. Yasuda, J. M. Macak, S. Berger, A. Ghicov, and P. Schmuki, "Mechanistic Aspects of the Self-Organization Process for Oxide Nanotube Formation on Valve Metals," *Journal of The Electrochemical Society*, vol. 154, no. 9, p. C472, 2007.

[24] U. H. Shah, K. M. Deen, H. Asgar, Z. Rahman, and W. Haider, "Understanding the mechanism of TiO_2 nanotubes formation at low potentials ($\leq$ 8 V) through electrochemical methods," *Journal of Electroanalytical Chemistry*, vol. 807, pp. 228-234, 2017.

[25] F. M. D'Heurle and J. M. E. Harper, "Note on the origin of intrinsic stresses in films deposited via evaporation and sputtering," *Thin Solid Films*, vol. 171, no. 1, pp. 81-92, 1989.

[26] A. J. Detor, A. M. Hodge, E. Chason, Y. Wang, H. Xu, M. Conyers, A. Nikroo, and A. Hamza," Stress and microstructure evolution in thick sputtered films, " *Acta Materialia*, vol. 57, no. 7, pp. 2055-2065, 2009.

[27] Y. K. V. Reddy, D. Mergel, S. Reuter, V. Buck, and M. Sulkowski, " Structural and optical properties of $BaTiO_3$ thin films prepared by radio-frequency magnetron sputtering at various substrate temperatures," *Journal of Physics D: Applied Physics*, vol. 39, no. 6, pp. 1161-1168, 2006.

[28] M. W. Liao and C. K. Chung, "The role and effect of residual stress on pore generation during anodization of aluminium thin films," *Corrosion Science*, vol. 74, pp. 232-239, 2013.

[29] A. Y. Chen, Y. Bu, Y. T. Tang, Y. Wang, F. Liu, X. F. Xie, and J. F. Gu," Deposition-rate dependence of orientation growth and crystallization of Ti thin films prepared by magnetron sputtering," *Thin Solid Films*, vol. 574, pp. 71-77, 2015.

[30] Y. Q. Fu, J. K. Luo, N. T. Nguyen, A. J. Walton, A. J. Flewitt, X. T. Zu, Y. Li, G. McHale, A. Matthews, E. Iborra, H. Du, and W. I. Milne," Advances in piezoelectric thin films for acoustic biosensors, acoustofluidics and lab-on-chip applications," *Progress in Materials Science*, vol. 89, pp. 31-91, 2017.

[31] J. Jaiswal, S. Mourya, G. Malik, S. Chauhan, R. Daipuriya, M. Singh, and R. Chandra, "Enhanced Optical Absorption of Ti Thin Film: Coupled Effect of Deposition and Post-deposition Temperatures," *The Journal of The Minerals, Metals & Materials Society (TMS)*, vol. 69, no. 11, pp. 2383-2389, 2017.

[32] M. Chinmulgund, R. B. Inturi, and J. A. Barnard, "Effect of Ar gas pressure on growth, structure, and mechanical properties of sputtered Ti, Al, TiAl, and Ti_3Al films," *Thin Solid Films*, vol. 270, no. 1-2, pp. 260-263, 1995.

[33] X. Pang, L. Zhang, H. Yang, K. Gao, and A. A. Volinsky, "Residual Stress and Surface Energy of Sputtered TiN Films," *Journal of Materials Engineering and Performance*, vol. 24, no. 3, pp. 1185-1191, 2015.

[34] Y. Tang, J. Tao, Z. Dong, J. T. Oh, and Z. Chen, "The formation of micrometer-long TiO_2 nanotube arrays by anodization of titanium film on conducting glass substrate," *Advances in Natural Sciences: Nanoscience and Nanotechnology*, vol. 2, no. 4, p. 045002, 2011.

[35] C. Lin, S. Chen, and L. Cao, "Anodic formation of aligned and bamboo-type TiO_2 nanotubes at constant low voltages," *Materials Science in Semiconductor Processing*, vol. 16, no. 1, pp. 154-159, 2013.

[36] R. Kojima, Y. Kimura, M. Bitoh, M. Abe, and M. Niwano, "Investigation of Influence of Electrolyte Composition on Formation of Anodic Titanium Oxide Nanotube Films," *Journal of The Electrochemical Society*, vol. 159, no. 11. pp. D629-D636, 2012.

[37] D. Regonini, A. Satka, A. Jaroenworaluck, D. W. E. Allsopp, C. R. Bowen, and R. Stevens, "Factors influencing surface morphology of anodized TiO_2 nanotubes," *Electrochimica Acta*, vol. 74, pp. 244-253, 2012.

[38] A. Stróż, G. Dercz, B. Chmiela, D. Stróż, and B. Łosiewicz, "Electrochemical Formation of Second Generation TiO_2 Nanotubes on Ti13Nb13Zr Alloy for Biomedical Applications," *Acta Physica Polonica A*, vol. 130, no. 4, pp. 1079-1080, 2016.

[39] H. Amani Hamedani, S. W. Lee, A. Al-Sammarraie, Z. R. Hesabi, A. Bhatti, F. M. Alamgir, H. Garmestani, and M. A. Khaleel, "Synthesis and Growth Mechanism of Thin-Film TiO_2 Nanotube Arrays on Focused-Ion-Beam Micropatterned 3D Isolated Regions of Titanium on Silicon," *ACS Applied Materials & Interfaces*, vol. 5, no. 18, pp. 9026-9033, 2013.

[40] S. Farsinezhad, A. Mohammadpour, M. Benlamri, A. N. Dalrymple, and K. Shankar, "The Morphology of TiO_2 Nanotube Arrays Grown from Atomically Peened and Non-Atomically Peened Ti Films," *Journal of Nanoscience and Nanotechnology*, vol. 17, no. 7, pp. 4936-4945, 2017.

[41] A. Apolinário, C. T. Sousa, J. Ventura, J. D. Costa, D. C. Leitão, J. M. Moreira, J. B. Sousa, L. Andrade, A. M. Mendes, and J. P. Araújo,"The role of the Ti surface roughness in the self-ordering of TiO_2 nanotubes: a detailed study of the growth mechanism," *Journal of Materials Chemistry A*, vol. 2, no. 24, pp. 9067-9078, 2014.